Proceedings of Coastal and Ocean Engineering in Korea (2000)
Vol. 11, pp. 140-148

Simulation of Wave-Induced Currents by Nonlinear Mild-Slope Equation and Comparison with PIV Measurements
비선형 완경사 방정식에 의한 연안류의 모의 및 PIV 관측결과와의 비교

Jung Lyul Lee[1], Chan Sung Park[2] and Sang Woo Han[1]
이정렬[1] · 박찬성[2] · 한상우[1]

1. INTRODUCTION

The nearshore currents are required for the preservation of coastal areas and the more pressing environmental problems since they cause sediments to be in suspension and transport the sediments into tranquil regions. Numerical models are often used to calculate current patterns formed around man-made or naturally caused changes around the coastal area. A prominent feature in the nearshore zone is the wave-induced current circulation. Two classes of approaches exist to simulate such wave-induced currents: (i) phase-averaged models that calculate large scale motions due to wave-induced forcing and (ii) models that resolve the instantaneous state of motion, such as models based on the nonlinear mild slope equations or the Boussinesq equations.

1.1 Phase-Averaged Approach

It is commonly accepted that the primary driving force for phase-induced currents is gradients in the radiation stress first introduced by Longuet-Higgins and Stewart (1961), which are defined as the excess momentum flux due to wave motion. The basic equations of mass and momentum are obtained through phase-averaged and depth-integrated approach. Modeling has advanced considerably from the earlier development by Noda et al. (1974) and Ebersole and Dalrymple (1979). Both of these earlier, models were driven by a wave refraction model with no current feedback. In recent years, Yoo and O'Connor (1986) developed a coupled wave-induced circulation model based upon what could be classified as a hyperbolic type wave equation; Yan (1987) and Winer (1988) developed their interaction models based upon parabolic approximation of the wave equation. All these models employed the depth-averaged or depth-integrated formulations. Recently, some models for determining the three dimensional currents have been proposed. De Vriend and Stive (1987), Lee (1993), and Kuroiwa et al. (1998) improved the nearshore circulation model by employing a quasi-three dimensional technique. This technique is very attractive to accommodate the surf zone in which the depth-averaged model is no longer valid. For the three dimensional nearshore currents, some models (Pechon and Teisson, 1994; Nobuoka et al., 1998) also have been developed in the surf zone. The Nobuoka's 3D model was developed by using the vertical distribution of radiation stress.

[1] 성균관대학교 토목환경공학과 (Dept. of Civil and Environmental Eng. , Sungkyunkwan University, Suwon Campus, Suwon 440-746, Korea)
[2] ㈜도화종합기술공사 항만부 (Dept. of Port and Coast Eng., Dohwa Consulting Engineers Co., Ltd. Seoul 135-780, Korea)

1.2 Nonlinear Wave Approach

The conventional models for wave-induced currents are based on a splitting of the phenomenon into a linear wave problem described by the mild-slope equation and a current problem described by the shallow water equations including radiation stress. Wave-current interaction effects such as current-induced refraction and wave blocking may be included in these systems by successive and iterative model executions.

More recently, however, a more direct approach to the problem has been proposed by Kabiling and Sato (1993) and Sorensen et al. (1994). The approach is accomplished by the use of a Boussinesq model which automatically includes the combined effects of wave-wave and wave-current interaction without need for inclusion of radiation stress. It is notable that the approach of using the radiation stress has the major restriction on the reflected wave existing condition since the conventional radiation stresses can be derived under the progressive wave field.

2. DIRECT PREDICTION BY NONLINEAR MILD-SLOPE EQUATION

A set of the governing equations used for dispersive wave-current in this study are given by Park(2000):

$$\frac{\partial^2 \eta}{\partial t^2} + \nabla \cdot \left[\left(\frac{CCg}{g} + \eta \right) \left(\frac{\partial \mathbf{u}_o}{\partial t} \right) \right] + \nabla \cdot \left(\mathbf{u}_o \frac{\partial \eta}{\partial t} \right) + \frac{\sigma^2 - k^2 CCg}{g} \left[\frac{1}{2} \mathbf{u}_o^2 + g\eta + \frac{3}{2} \left(\frac{\partial \eta}{\partial t} \right)^2 \right] + 2 \frac{\sigma^4}{g} \eta^2 = 0 \tag{1}$$

$$\frac{\partial \mathbf{u}_o}{\partial t} + g \nabla \eta + \mathbf{u}_o \cdot \nabla \mathbf{u}_o + \frac{3}{2} \nabla \left(\frac{\partial \eta}{\partial t} \right)^2 = 0 \tag{2}$$

where η is the free surface displacement, $\mathbf{u}_o$ the horizontal velocity vector defined at the mean water level, C and Cg are the local phase speed and the group velocity, respectively, g the gravitational acceleration, k the wave number, and σ the angular frequency.

The governing equations (1) and (2) are solved by using a fractional step method in conjunction with the approximate factorization techniques leading to the implicit finite difference schemes. The implicit scheme turns out that the implicit scheme accelerates the convergence of numerical calculations for the steady-state solutions.

We used the Miche's criterion (Miche, 1951) because the breaking wave model is simple and accurate enough, and guarantees stability. For the mass conservation, the broken mass due to wave breaking is consequently passed on the next step elevation at each grid.

3. PHASE-AVERAGED APPROACH

The second model is based on results obtained by Lee and Wang (1993) in the depth-integrated form. The continuity equation :

$$\frac{\partial \eta_c}{\partial t} + \frac{\partial}{\partial x}(Q_x + M_x) + \frac{\partial}{\partial y}(Q_y + M_y) = 0 \tag{3}$$

where η_c is the mean water level, Q_x and Q_y are the x and y components of the mean flow rate integrated from bottom to mean water level, respectively, as defined below;

$$Q_x = \int_{-h}^{\eta_c} u dz \quad \text{and} \quad Q_y = \int_{-h}^{\eta_c} v dz$$

and M_x and M_y are the phase-averaged flow rate induced by the wave motion, which are evaluated as

$$M_x = \frac{gH^2 k_x}{8\sigma} \quad \text{and} \quad M_y = \frac{gH^2 k_y}{8\sigma}$$

In the steady state, the depth-integrated total mass flux has to be zero.

The x-directional modified momentum equation:

$$\frac{\partial Q_x}{\partial t} + \frac{\partial}{\partial x}\left(\frac{Q_x^2}{h+\eta_c} \right) + \frac{\partial}{\partial y}\left(\frac{Q_x Q_y}{h+\eta_c} \right) + \frac{1}{\rho}\frac{\partial S_{xx}}{\partial x} + \frac{1}{\rho}\frac{\partial S_{yx}}{\partial y} + g(h+\eta_c)\frac{\partial \eta_c}{\partial x} + \frac{\tau_{Bx}}{\rho} = 0 \tag{4}$$

The y-directional modified momentum equation:

$$\frac{\partial Q_y}{\partial t}+\frac{\partial}{\partial x}\left(\frac{Q_x Q_y}{h+\eta_c}\right)+\frac{\partial}{\partial y}\left(\frac{Q_y^2}{h+\eta_c}\right)+$$
$$\frac{1}{\rho}\frac{\partial S_{xy}}{\partial x}+\frac{1}{\rho}\frac{\partial S_{yy}}{\partial y}+g(h+\eta_c)\frac{\partial \eta_c}{\partial y}+\frac{\tau_{By}}{\rho}=0 \quad (5)$$

where,

$$S_{xx}=E\left[n(\cos^2\theta+1)-\frac{1}{2}\right]$$

$$S_{xy}=S_{yx}=E[n\sin\theta\cos\theta]$$

$$S_{yy}=E\left[n(\sin^2\theta+1)-\frac{1}{2}\right]$$

$$E=\frac{1}{8}\rho g H^2$$

where n is the ratio of the group velocity Cg to the phase speed C.

The bottom friction consists of bottom friction due to viscous and streaming flows:

$$\tau_B=\overline{\tau_{B,bf}}+\overline{\tau_{B,strm}}$$
$$=\rho|u_{orb}|\left(F_{bf}U_B+F_{strm}U_{strm}\right) \quad (6)$$

where, F_{bf} is the bottom friction factor, while F_{strm} is the friction factor due to the streaming flow. And $|u_{orb}|=gH/2C$ as the orbital velocity at the bottom and U_{strm} is the streaming current measured at the bootm under progressive waves.

The lateral shear stress is added to the momentum equation as

$$\tau_l=-\rho\left[\varepsilon_y\frac{\partial u}{\partial y}+\varepsilon_x\frac{\partial v}{\partial x}\right] \quad (7)$$

The mixing length coefficient, ε_x is assumed to be constant here for the practical use, instead of values proportional to the distance from the shoreline, $|x|$.

The governing equations (3), (4) and (5) are also solved by using a fractional step method in conjunction with the approximate factorization techniques leading to the implicit finite difference schemes.

4. PIV EXPERIMENTS

Most of former experimental works were focused on the measurement of the water surface displacements without taking the flow patterns around the obstacle into account. Although it was expected that a man-made structure permits the nearshore circulation, it was rarely measured how strong currents can be formed, particularly in the case of breaking waves. Recently, a several image-based system allows to visualize the flow field near a breakwater with detailed information about the flow distributions.

4.1 PIV

Particle Image Velocimetry(PIV) is a superior flow visualization technique for providing an instantaneous, non-intrusive insight into velocity field distributions with qualitative and quantitative information. It offers many advantages over other conventional velocimetries, such as laser Doppler anemometry and hot-wire anemometry.

PIV principals are as follows. First of all, the flow field plane section of a flow containing neutrally buoyant particles is illuminated, typically by laser light. And then illuminated particles within flow field are captured by CCD camera or camcorder. Finally, an image analysis technique is used to determine the particle displacements in time interval of sequential images to visualize the velocity field.

Basic concept of PIV is a comparison of two successive images during small interval time, Δt are divided into small area called interrogation area and searching area as shown in Fig. 1. Interrogation and searching area are compared in the two successive images using the cross correlation algorithm. The Cross Correlation PIV assumes the velocity relatively uniform within a search region and no change in the flow pattern between successive two images. PIV has restrictive spatial resolution because velocities are assumed uniform within interrogation area. A spatial shift caused by the fluid flow may be observed from interrogation area to the searching area. Generally a side length of searching area, M is a little larger than the drift by the greatest velocity in the whole flow field.

It is good to decide what is the size of measurement area and the greatest velocity with knowledge. If time interval, Δt is fixed and to increase velocity range, interrogation area must be increased. If the side length includes N pixel, FFT calculation takes time in proportion to $2N\log N$ but if the side length includes 2^n pixel, FFT calculation takes time in proportion to $N\log N$. So generally, the interrogation area of 32×32 or 64×64 pixels are used. For application of the FFT, it is suggested limiting the maximum displacements between 1/4 and 1/3 of the interrogation area dimensions.

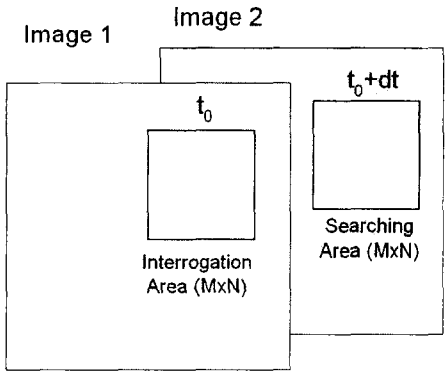

Figure 1. Interrogation area and searching area

One of determination of centroid, Willert and Gharib (1991) provides sub-pixel accuracy. In controlled experiments, they found a minimum uncertainty value of 0.01 pixels. However, in practice the uncertainty may be an order of magnitude higher. Parabolic curves are fit through the peak and each of the two neighboring data points in both the vertical and horizontal directions.

The distances from the origin to the location of the maximum of these parabolas determine the displacement vector to sub pixel accuracy. By dividing the displacement vector by the known time difference between frames, the velocity vector is found. In this experiment, the summit point is calculated by quadratic function interpolation.

4.2 PIV Setup

A schematic description of the experiment setup is shown in Fig. 2, which consists of image capturing system. The fluid velocity was obtained using optical and digital processing techniques.

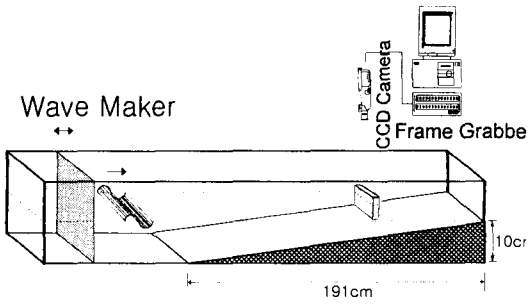

Figure 2. Schematic description of the experiment setup

Under the wave breaking, most of particles are deviated from the image width due to the wave-induced turbulent flow so that the small pieces of plastic ball of about 5 *mm* diameter are used as particles under the sunlight rather than a laser beam in order to capture all particles of the section.

The displacement fields were recorded by a SMD-1M60 CCD camera (SMD co.) with a 50 *mm* Nikkor lens (Nikon Co.). The image data were stored digitally using an AM-MTD (Imaging Technology) frame grabber, set to record the spatial resolution of 1024×1024 pixels gray-level images from the CCD camera.

To extract current velocity distributions from the successive images, Matlab by the MathWorks Inc., a manipulation software package, was used to process the images on the Pentium Personal Computer. In this experiment, the interrogation area was used 128×128 pixel. The scanned area corresponds to a square region 896×1024 pixel. And flow images were taken in 1/13 *sec* interval.

4.3 Experimental Setup

The experiment was conducted in a Coastal-Hydraulics Laboratory wave flume of Sungkyunkwan University, in order to verify the numerical results of wave-induced currents. The wave flume of 50 *cm* deep, 40 *cm* wide, and 12 *m* long consists of a wave generator and beach zones. The bottom and side walls of the flume are glass to allow easy optical access. The regular waves were generated by a piston-type wave paddle and the beach slope of 1/19 was set at the other end of the wave flume.

The wave flume was decorated with the data acquisition system accessing the wave profile signals from the wave gages. Gages were connected with amplifier for increasing analog signals. Then the DaqBoard 100A (DaqBoard), A/D converter, changes conditioned signals into corresponding digital numbers saved as ASCII format.

For an example of the capabilities of the numerical model, computations will be compared with the physical experiments carried out in this study. Physical experiments were accomplished for two cases. Experimental conditions consist of same wave conditions for two different experimental setups, respectively. Wave conditions are T=0.8sec, Hi= 2*cm* Ur=10.05 and steepness= 0.0282.

The layouts of two different experimental configurations are illustrated in Fig. 3 and 4 showing the locations of the measurement stations and detailed geometry of the flume. The exposed breakwater was placed to the left half of the wave

tank looking in the direction of the wave propagation, while the submerged breakwater was placed to the left side.

For the Case 1 as shown in Fig. 3, wave gages 1, 2 and 3 were located at x=41cm, x=81cm and x=121cm measured shoreward from the toe of slope, respectively. The measuring section was located about 10.5 cm apart from the nearer sidewall.

The Case 2 as for the submerged breakwater are as shown in Fig. 4. Wave gages 1, 2 and 3 were located at x=-21.5cm, x=0cm (center) and x=12.5cm measured shoreward from the center of submerged breakwater, respectively. The squared submerged breakwater is impermeable and 1.1 cm high and 15 cm long.

4.4 PIV System Test

The two successive images shown in Fig. 5 are examples taken in 1/13 sec interval by CCD camera under the wave condition of H_i = 2cm, and T = 0.8s, and the resulting velocity vectors are plotted in Fig. 6. The threshold level used for image treatment was 70 and the AOI of 128 pixel was used.

5. COMPARISON OF PIV EXPERIMENTS AND NUMERICAL RESULTS

Model results from both nonlinear wave phase approach and phase-averaged radiation stress approach, and PIV experiments are compared with images of same size as shown in Figs. 7-12, respectively. The radiation stress approach was done with no current feedback.

It is found in each figure of Case 1 that a closed circulation flow is generated behind the breakwater. The nonlinear wave phase model and the experimental data were time-averaged over last several wave periods. An observed image area is of 40cm width and 46.3cm length as shown in Fig. 3. Both side boundaries of the image are impermeable glass wall but the upper and lower boundaries are open so as to permit vectors crossing with them. As shown in Figs. 7 and 8, both model results show good agreement each other. However, the observed results show overall agreement in circulation pattern with model results but as shown in experiments by PIV system (Fig. 9) the strong seaward currents behind a breakwater do not appear in both model results. The major difference is thought to happen since both models do not take into account the strong shoreward mass flux cast near crest levels as waves break. Therefore, such effect should be taken into account for better accuracy.

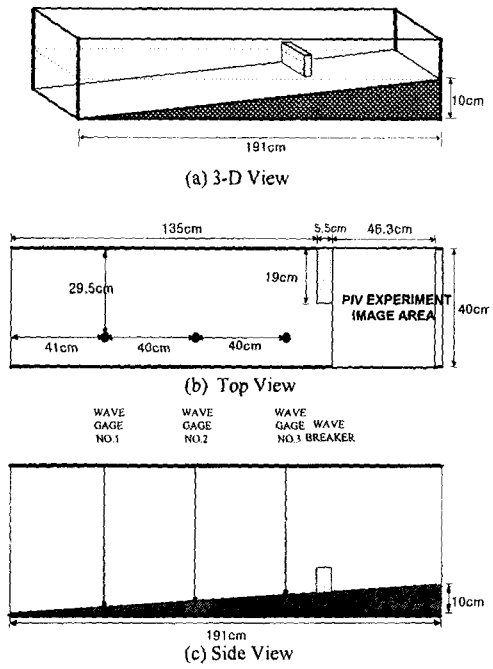

Figure 3. Physical layout of experiment: (a) 3-D view, (b) top view, (c) side view

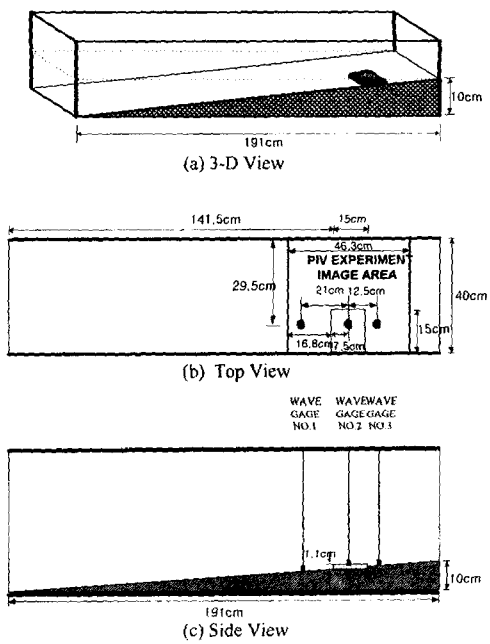

Figure 4. Physical layout of experiment: (a) 3-D view, (b) top view, (c) side view

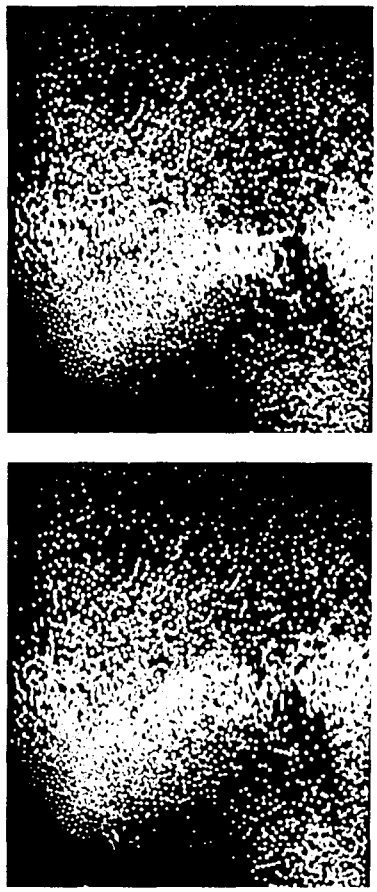

Figure 5. Particle image taken in 1/13 *sec* interval under the wave condition of Hi=2 *cm*, and T=0.8 *s*, Case 1. (threshold level 70 given)

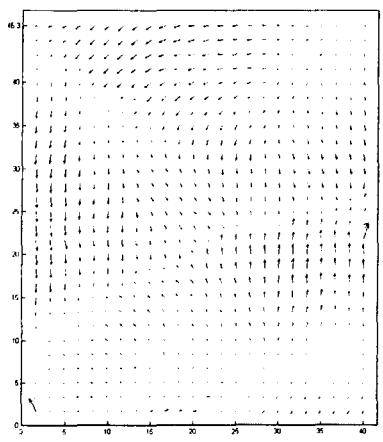

Figure 6. Instantaneous velocity vectors obtained from two successive images in Figure 5

As shown in Fig. 9, the current vectors depicted by PIV experiments appear to violate the mass balance though the overall performance is satisfactory. The primary reason is thought that the image capturing time interval is too wide to keep up with the fast moving shoreward orbital motions.

The experiments are also performed for a submerged breakwater. Two models and one PIV experiment (Case 2) were also carried out. The results are shown in Figs. 10-12, respectively. The onshore currents over a submerged breakwater by PIV measurements were underestimated when compared with eye observation. At this moment, therefore, the prediction capability by nonlinear wave model for the submerged breakwater case is verified only through the classical phase-averaged radiation stress approach.

6. CONCLUSIONS

Comparison was accomplished for three kinds of results from nonlinear wave phase approach and phase-averaged radiation stress approach, and PIV experiments. The wave-induced currents in nonlinear wave phase approach were determined by integrating the depth-integrated velocities over wave periods and then dividing it by the number of wave period taken and the local mean water depth. In the present study for comparison, the phase-averaged radiation stress approach was done with no current feedback.

Results from both models showed good agreement each other. As compared with the observed results, both numerical approaches yielded the underestimated strength of current vectors. The difference is thought to happen since both models did not take into account the strong shoreward mass flux cast near crest levels as waves break. Therefore, such effect should be taken into account for better accuracy. The current vectors depicted by PIV experiments violate the mass balance though the overall pattern was satisfactory. In addition, the onshore currents over a submerged breakwater by PIV measurements were under-estimated when compared with eye observation. The primary reason is thought that the image capturing time interval was too wide to keep up with the fast moving shoreward orbital motions well. For the submerged breakwater cases, in particular, the limitation of PIV appeared to be significant. Therefore, the nonlinear wave model was verified only through the classical phase-averaged radiation stress approach. However, we offered the errorous physical results to show the limitation of the present

PIV technique which can be overcome by the mechanical choking to shorten the time interval, or hardware/software in the further for accessing images in shorter interval.

Another weakness in the present PIV measurement is that the mean position of particles used for the image capture were observed biased to the bottom due to little higher specific gravity than unit.

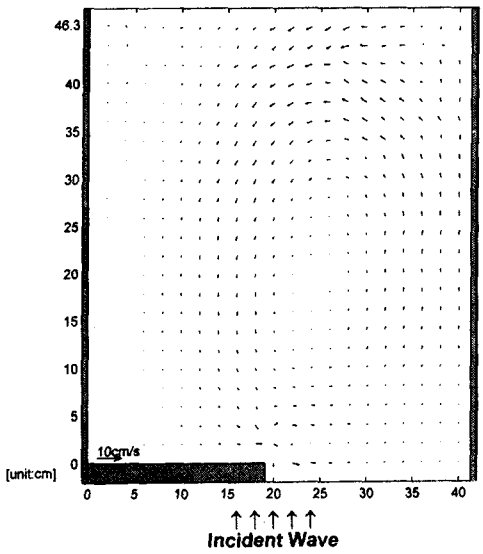

Figure 7. Current vectors by nonlinear wave approach

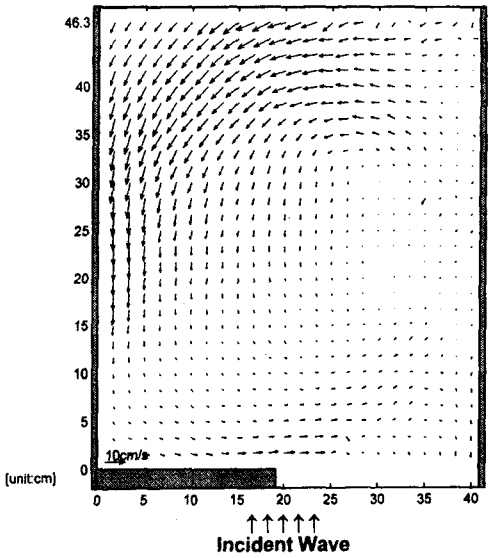

Figure 9. Current vectors by physical experiments Using a PIV system

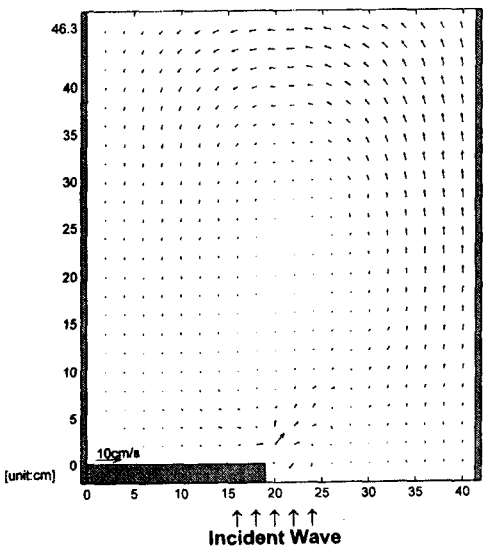

Figure 8. Current vectors by radiation stress approach

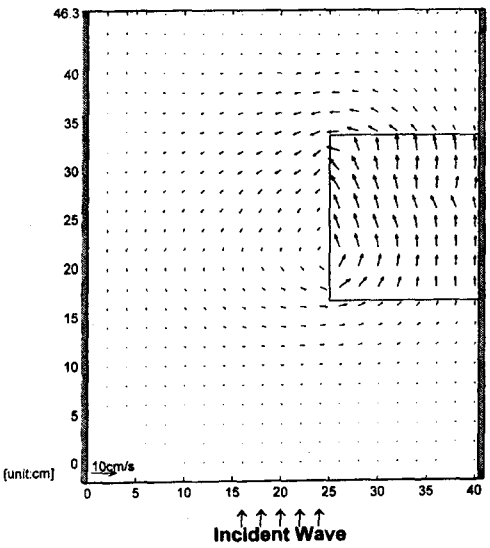

Figure 10. Current vectors by nonlinear wave approach

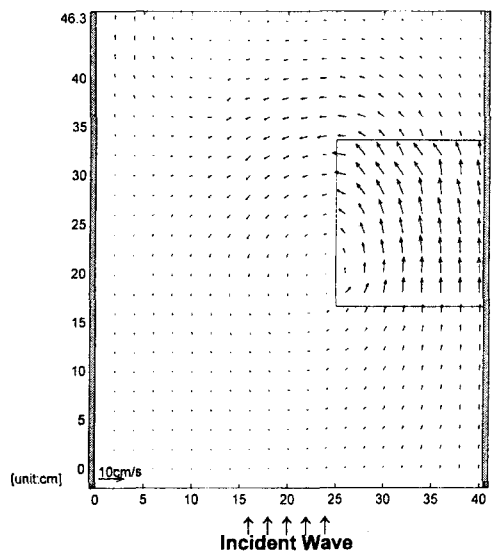

Figure 11. Current vectors by radiation stress approach

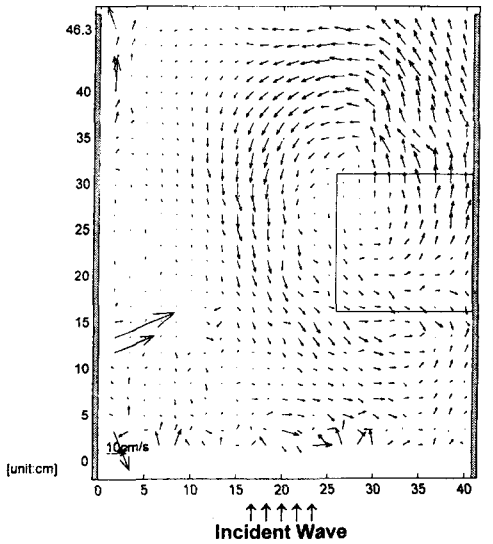

Figure 12. Current vectors by physical experiments using a PIV system

REFERENCES

Berkhoff, J.C.W., 1972. Computation of combined refraction-diffraction, *Proc. 13rd Int. Conf. Coastal Engrg.*, ASCE, 471-490.

Chorin, A.J., 1968. Numerical solution of the Navier-Stokes equations, *Math. Comput.*, 22:745-762.

De Vriend, H.J., and Stive, M.J.F., 1987. Quasi-3D modeling of nearshore currents, Coastal Eng., 11: 565-601.

Ebersole, B.A., and Dalrymple, R.A., 1979. A numerical model for nearshore circulation including convective accelerations and lateral mixing, Ocean Engineering Report No. 21, Dept. of Civil Eng., Univ. of Delaware, Newark, Delaware.

Kabiling, M.B., and Sato, S., 1993. Two-dimensional nonlinear dispersive wave-current and three-dimensional beach deformation model, *Coastal Engrg., in Japan,* 36:196-212.

Kuroiwa, M., Noda, H., and Matsubara, Y., 1998. Application of a quasi-three dimensional numerical model to nearshore currents, *Proc. 26th Int. Conf. Coastal Engrg.*, ASCE, 815-828.

Lee, J.L., 1993. Wave-current interaction and quasi-three-dimensional modeling in nearshore zone, Ph.D dissertation, Coastal and Oceanographic Engineering Department, Unv. of Florida, Gainesville.

Lee, J.L. and Wang, H. 1993. Mathematical model for 3-dimensional circulation in surf zone, *J. the Korean Society of Coastal and Ocean Engineers*, 5(4): 369-383

Longuet-Higgins, M.S., and Stewart, R.W., 1961. The changes in amplitude of short gravity waves on steady non-uniform currents, *J. Fluid Mech.*, 10:529-549.

Miche, R., 1951. The reflecting power of maritime works exposed to action of the waves, Annals of the Highway Dept., National Press, France.

Nobuoka, H., Mimura, N., and Kato, H., 1998. Three-dimesional nearshore currents model based on vertical distribution of radiation stress, *Proc. 26th Int. Conf. Coastal Engrg.*, ASCE, 829-842.

Noda, D., Sonu, C.J., Rupert, V.C., and Collins, J.I., 1974. Nearshore circulation under sea breeze conditions and wave-current interactions in the surf zone, Tetra Tech Report TC-149-4.

Pechon, P., and Teisson C., 1994. Numerical modeling of three-dimensional wave-driven currents in the surf-zone, *Proc. 24th Int. Conf. Coastal Engrg.*, ASCE, 2503-2512.

Park, C.S., 2000. Physical experiments and numerical simulations of 3-D morphological evolution using nonlinear mild-slope equation, MS thesis, Dept. of Civil Engineering,

Sungkyunkwan Unv., Seoul.

Peregrine, D.H., 1967. Long waves on a beach, *J. Fluid Mech.*, 27(4):815-827.

Peregrine, D.H., 1974. Discussion of : A numerical simulation of the undular hydraulic jump, by M.B. Abbott and G.S. Rodenhuis., *J.Hydraul. Res.*, 12(1):141-157.

Rosenfeld, M.,Kwak, D., and Vinokur, M. 1991. A fractional step solution mehod for the unstead incompressible Navier-Stoke equations in generalized coordinate system, J. Comp. Physics, 94: 102-137.

Sorensen, O.R., Schäffer, H.A., Madsen, P.A., and Deigaard, R., 1994. Wave breaking and induced nearshore circulations, *Proc. 24th Int. Conf. Coastal Engrg.*, 2583-2594

Yan, Y., 1987. Numerical modeling of current and wave interaction on an inlet-beach system, Techincal Report No. 73, Coastal and Oceanographic Engineering Department, Univ. of Florida, Gainesville.

Yoo, D., and O'Connor, B.A. 1986. Mathematical modeling of wave-induced nearshore circulations, *Proc, 20th Int. Conf. Coastal Engrg.*, ASCE, 1667-1681.

Willert, C. E., and Gharib, M., 1991. Digital particle image velocimetry, *Experiments in Fluids*, 10:181-193.

Winer, H.S., 1988. Numerical modeling of wave-induced currents using a parabolic wave equation, Ph.D dissertation, Coastal and Oceanographic Engineering Department, Univ. of Florida, Gainesville.